Contents

1 The Great Acceleration: Data Sources

1.1 Socio-economic indicators

Indicator	Description	Unit	Source(s)
1. World population	Global population data according to Our World in Data, based on data from HYDE v3.3 for 1750-1799, Gapminder v7 for 1800-1949, UN World Urbanization Prospects (WUP) for 1950 to 2023, and Gapminder Systema Globalis as an additional source for former countries (Yugoslavia, USSR, etc.), with major processing by Our World in Data.	Billion	Our World in Data (2024). *Population, 10,000 BCE to 2023*. https://ourworldindata.org/grapher/population (accessed in 2026). Klein Goldewijk (2023). *History Database of the Global Environment 3.3*. Utrecht University https://doi.org/10.24416/UU01-AEZZIT Gapminder v7 (2022). https://www.gapminder.org/data/documentation/gd003/ United Nations, Department of Economic and Social Affairs, Population Division (2024). World Population Prospects 2024, Online Edition. Gapminder - Systema Globalis (2023). https://github.com/open-numbers/ddf--gapminder--systema_globalis
2. Real GDP	Global real Gross Domestic Product (GDP) in year 2011 US dollars according to the Maddison Project Database 2023.	Trillion of real 2011 U.S. dollars	Bolt & van Zanden (2024). *Maddison Project Database 2023*. DataverseNL, V1. https://doi.org/10.34894/INZBF2 Bolt & Van Zanden (2025). Maddison-style estimates of the evolution of the world economy: A new 2023 update. *J. Econ. Surv.* **39**, 631–671.
3. Foreign direct investment	Global foreign direct investment in current (accessed 2026) US dollars. Data before 1990 follows Steffen et al. (2015), based on International Monetary Fund (IMF) data from 1948–1969 and United Nations Conference on Trade and Development (UNCTAD) data from 1970–1989, both accessed in 2013, and adjusted for inflation. Data from 1990 to 2023 is from UNCTAD, accessed in 2026.	Trillion of 2025 U.S. dollars per year	Steffen et al. (2015). The trajectory of the Anthropocene: The Great Acceleration. *Anthr. Rev.* **2**, 81–98. IMF (n.d.). *International Monetary Fund eLibrary Data*. https://www.imf.org/ (accessed in 2013). UNCTAD (n.d.). *United Nations Trade and Development Data Hub*. https://unctadstat.unctad.org/datacentre/dataviewer/US.FdiFlowsStock (accessed in 2013 and 2026).

Indicator	Description	Unit	Source(s)
4. Urban population	Global urban population data. Data from 1750-1949 follows the HYDE database v3.5. Data from 1950 to 2025 follows Our World in Data, based on data from the UN World Urbanization Prospects (WUP) with minor processing by Our World in Data. To remove the small offset between the two sources at their junction, the HYDE segment is scaled by a constant factor of 0.976581 (the ratio of the WUP 2025 to HYDE 3.5 values at 1950, 717.97 M / 735.18 M), making the series continuous at the 1950 splice.	Billion	Klein Goldewijk (2025). *HYDE data for the Global Carbon Budget (2025) 3.5*. Utrecht University. `https://doi.org/10.24416/UU01-F45D44` (accessed in 2026). Our World in Data (2026). *Number of people living in urban and rural areas, World*. `https://ourworldindata.org/grapher/urban-and-rural-population` (accessed in 2026). United Nations, Department of Economic and Social Affairs, Population Division (2025). *World Urbanization Prospects: The 2025 Revision, Online Edition*. POP/DB/WUP/Rev.2025/F14
5. Primary energy use	World primary energy use according to Our World in Data, based on data from the Energy Institute (EI) and Smil (2017) with major processing by Our World in Data.	Exajoule per year	Our World in Data (2024). *Global direct primary energy consumption*. `https://ourworldindata.org/grapher/global-primary-energy` (accessed in 2026). Energy Institute (2024). *Statistical Review of World Energy.* `https://www.energyinst.org/statistical-review` Smil (2017). *Energy Transitions: Global and National Perspectives* (Appendix A). Santa Barbara, CA: Praeger, an imprint of ABC-CLIO, LLC.
6. Fertilizer consumption	Global fertilizer (nitrogen, phosphate and potassium) consumption according to data from the Food and Agriculture Organization of the United Nations (FAO). Data prior to 1961 were retained as reported in Steffen et al. (2015), based on personal correspondence with Olivier Rousseau from the International Fertilizer Industry Association (IFA).	Million tonnes per year	Steffen et al. (2015). The trajectory of the Anthropocene: The Great Acceleration. *Anthr. Rev.* **2**, 81–98. FAO (n.d.). *FAOSTAT statistical database: Fertilizers by Nutrient.* `https://www.fao.org/faostat/en/#data/RFN` (accessed in 2026).
7. Large dams	Global total number of large dams built since 1900 according to data from the International Commission on Large Dams (ICOLD) as extracted from Figure 1 in Perera et al. (2021). Large dams are defined as having a minimum height of 15 metres above the foundation, or 5–15 metres height and impounding more than 3 million cubic metres.	Thousand dams	Perera et al. (2021). *Ageing Water Storage Infrastructure: An Emerging Global Risk 11.* United Nations University (UNU). ICOLD (2020). *World Register of Dams: General Synthesis.* `https://www.icold-cigb.org/GB/world_register/general_synthesis.asp` (accessed in 2020).

Indicator	Description	Unit	Source(s)
8. Water use	Global water use. Data from 1900 to 1999 follows Steffen et al. (2015), based on estimations from Flörke et al. (2013), aus der Beek et al. (2010), and Alcamo et al. (2003), using the WaterGAP model. AQUASTAT data from the Food and Agriculture Organization of the United Nations (FAO) is used from 2000 to 2022.	Thousand km^3 per year	Steffen et al. (2015). The trajectory of the Anthropocene: The Great Acceleration. *Anthr. Rev.* **2**, 81–98. Flörke et al. (2013). Domestic and industrial water uses of the past 60 years as a mirror of socio-economic development: A global simulation study. *Glob. Environ. Change* **23**, 144–156. aus der Beek et al. (2010). Modelling historical and current irrigation water demand on the continental scale: Europe. *Adv. Geosci.* **27**, 79–85. Alcamo et al. (2003). Development and testing of the WaterGAP 2 global model of water use and availability. *Hydrol. Sci. J.* **48**, 317–337. FAO (n.d). *AQUASTAT: FAO's Global Water Information System.* `https://data.apps.fao.org/aquastat/` (accessed 2026).
9. Paper production	Global paper production (paper and paperboard) according to data from the Food and Agriculture Organization of the United Nations (FAO).	Million tonnes per year	FAO (n.d.). *FAOSTAT statistical database: Forestry Production and Trade.* `https://www.fao.org/faostat/en/#data/FO` (accessed in 2026).
10. Global infrastructure agreements	Number of global infrastructure agreements according to Haner (2023), based on an analysis of the Consolidated Treaty Series (CTS), the League of Nations Treaty Series (LNTS), and the United Nations Treaty Series (UNTS).	Thousand agreements	Haner (2023). *Organizing peace: An algorithmic analysis of four centuries of international law and the decline of war* (Doctoral dissertation, Northeastern University). ProQuest LCC Publishing.
11. Telecommunications	Global sum of fixed landlines and mobile phone subscriptions. Landline data are based on Canning (1998) for 1950-1989 and data from the United Nations Statistics Division (UNSD) from 1990-2022. Mobile phone subscription data are based solely on UNSD data from 1990-2022.	Billion telephone subscriptions	Canning (1998). A database of world stocks of infrastructure: 1950–1995. *The World Bank Economic Review*, 12(3), 529–548. UNSD (2014). *UNdata database: Landline telephones and mobile phones.* `http://data.un.org/Data.aspx?q=telephones&d=MDG&f=seriesRowID%3a779` and `http://data.un.org/Data.aspx?q=cellular&d=ITU&f=ind1Code%3aI271` (accessed 2026)
12. Transistors per microprocessor	Number of transistors per microprocessor according to data from Rupp (2022), processed by Our World in Data. A data point was added with the value 1 in 1947 for the first transistor.	Billion transistors	Rupp (2022). *Microprocessor Trend Data.* `https://github.com/karlrupp/microprocessor-trend-data` (accessed in 2023). Processed by Our World in Data: `https://ourworldindata.org/grapher/transistors-per-microprocessor`

Table 1.1: Trends from 1750 to 2025 in indicators for socio-economic development.

1.2 Earth System indicators

Indicator	Description	Unit	Source(s)
1. Carbon dioxide	Global carbon dioxide concentration according to data from the Indicators of Global Climate Change 2025.	Parts per million	Smith et al. (2025). *Indicators of Global Climate Change 2025.* `https://zenodo.org/records/20708818` (accessed in 2026).

Indicator	Description	Unit	Source(s)
2. Nitrous oxide	Global nitrous oxide concentration according to data from the Indicators of Global Climate Change 2025.	Parts per billion	Smith et al. (2025). *Indicators of Global Climate Change 2025.* `https://zenodo.org/records/20708818` (accessed in 2026).
3. Methane	Global methane concentration according to data from the Indicators of Global Climate Change 2025.	Parts per billion	Smith et al. (2025). *Indicators of Global Climate Change 2025.* `https://zenodo.org/records/20708818` (accessed in 2026).
4. Stratospheric ozone	Maximum percentage total column ozone decline over Halley, Antarctica during October, using 305 DU, the average October total column ozone for the first decade of measurements, as a baseline.	Percentage	Shanklin, British Antarctic Survey (n.d.). Antarctic Ozone. `https://legacy.bas.ac.uk/met/jds/ozone/index.html#data` (accessed in 2026).
5. Surface temperature	Global surface temperature anomaly according to the HadCRUT5 analysis by the Climate Research Unit (University of East Anglia and NCAS), and the Hadley Centre (UK Met Office). Combined land and ocean observations, relative to 1961-1990.	Degrees Celsius	Morice et al. (2021). An updated assessment of near-surface temperature change from 1850: The HadCRUT5 data set. *Journal of Geophysical Research: Atmospheres*, **126** (e2019JD032361). Dataset version 5.1.0.0 retrieved from: `https://crudata.uea.ac.uk/cru/data/temperature/#sciref` (accessed in 2026).
6. Ocean acidification	Ocean acidification expressed as global mean surface ocean hydrogen ion concentration from a model-data fusion product (using 14 models from CMIP6) based on observations until 2014 and thereafter SSP2-4.5.	nmol kg^{-1}	Jiang et al. (2023). Global Surface Ocean Acidification Indicators From 1750 to 2100. *J. Adv. Model. Earth Syst.* **15**.
7. Marine fish capture	Global marine fishes capture production according to data from the Food and Agriculture Organization of the United Nations (FAO).	Million tonnes per year	FAO (n.d.). *Fishery and aquaculture statistics: Capture production quantity.* `https://www.fao.org/fishery/statistics-query/en?dataset=capture&timeseries=capture_quantity` (accessed in 2026).
8. Shrimp aquaculture	Global aquaculture shrimp production according to data from the Food and Agriculture Organization of the United Nations (FAO).	Million tonnes per year	FAO (n.d.). *Fishery and aquaculture statistics: Aquaculture production quantity.* `https://www.fao.org/fishery/statistics-query/en?dataset=aquaculture&timeseries=aquaculture_quantity` (accessed in 2026).
9. Nitrogen to coastal zone	Model-calculated human-induced perturbation flux of nitrogen into the coastal margin (riverine flux, sewage and atmospheric deposition). The source remains unchanged from Steffen et al. (2015).	Million tonnes per year	Steffen et al. (2015). The trajectory of the Anthropocene: The Great Acceleration. *Anthr. Rev.* **2**, 81–98. Mackenzie et al. (2002). Century-scale nitrogen and phosphorus controls of the carbon cycle. *Chemical Geology*, **190**, 13–32.

Indicator	Description	Unit	Source(s)
10. Tropical forest loss	Loss of tropical forests compared with 1700. Data for 1700 and from 1750 to 1992 are from Pongratz et al. (2008), based on reconstructions of land use and land cover. From 1993 to 2022, data from the Copernicus Climate Change Service (C3S) is used and is evaluated as the loss relative to 1992 (to avoid discontinuities at the transition from modeled to remote-sensing based data).	Percentage	Steffen et al. (2015). The trajectory of the Anthropocene: The Great Acceleration. *Anthr. Rev.* **2**, 81–98. Pongratz et al. (2008). A reconstruction of global agricultural areas and land cover for the last millennium. *Global Biogeochemical Cycles, 22*(4), GB3018. Copernicus Climate Change Service (2019). *Land cover classification gridded maps from 1992 to present derived from satellite observation.* `https://doi.org/10.24381/cds.006f2c9a` (accessed in 2024).
11. Domesticated land	Increase in agricultural land area, including cropland and pasture as a percentage of total land area. Data from 1750 to 1960 are based on reconstructions of land use from Pongratz et al. (2008). From 1961 to 2022, data is from the Food and Agriculture Organization of the United Nations (FAO).	Percentage	Steffen et al. (2015). The trajectory of the Anthropocene: The Great Acceleration. *Anthr. Rev.* **2**, 81–98. Pongratz et al. (2008). A reconstruction of global agricultural areas and land cover for the last millennium. *Global Biogeochemical Cycles, 22*(4), GB3018. FAO (n.d.). *FAOSTAT statistical database:Land Use.* `https://www.fao.org/faostat/en/#data/RL` (accessed in 2026).
12. Terrestrial biosphere degradation	Percentage loss of terrestrial mean species abundance relative to abundance in undisturbed ecosystems as an approximation for degradation of the terrestrial biosphere. The data follows Steffen et al. (2015) and is based on Alkemade et al. (2009) and ten Brink et al. (2010).	Percentage	Steffen et al. (2015). The trajectory of the Anthropocene: The Great Acceleration. *Anthr. Rev.* **2**, 81–98. Alkemade et al. (2009). GLOBIO3: A Framework to Investigate Options for Reducing Global Terrestrial Biodiversity Loss. *Ecosystems* **12**, 374–390. ten Brink et al. (2010). Global MSA baseline scenarios. In: *Rethinking global biodiversity strategies: Exploring structural changes in production and consumption to reduce biodiversity loss.* Netherlands Environmental Assessment Agency (PBL). The Hague/Bilthoven.

Table 1.2: Trends from 1750 to 2025 in indicators for the structure and functioning of the Earth System.

2 PB: Freshwater Change

Additional information on the global risk map of Earth's freshwater systems (I) – Blue water.

This map shows boundary transgression at river basin scale for major basins [1] of the world (n = 268). Transgression is based on the control variable, streamflow, with values potentially ranging from within the Safe Operating Space (green) to the Zone of Increasing Risk (yellow/orange), and extending to the High Risk Zone (red/purple). At the global scale, the high risk boundary (50%) is beyond the PB (12.9%) by a factor of 2.9, the current status (22.6%) transgresses the PB by a factor of 0.75, while the baseline state (10.3%) was below the PB by a factor of -0.20. Each basin has its specific safe level (evaluated similarly as the global safe level), and the risk level of each basin is determined by scaling its relative transgression factor with the global transgression factor (0.75). Basins depicted in the darkest shade of orange especially contribute to the global transgression, with regional land area deviations higher than the global factor. Based on data from [2].

Additional information on the global risk map of Earth's freshwater systems (I) – Green water.

This map shows boundary transgression at river basin scale for major basins [1] of the world (n = 268). Transgression is based on the control variable, root zone soil moisture, with values potentially ranging from within the Safe Operating Space (green) to the Zone of Increasing Risk (yellow/orange), and extending to the High Risk Zone (red/purple). At the global scale, the high risk boundary (50%) is beyond the PB (12.4%) by a factor of 3.0, the current status (22.0%) transgresses the PB by a factor of 0.77, while the baseline state (9.8%) is below the PB by a factor of -0.21. Each basin has its specific safe level (evaluated similarly as the global safe level), and the risk level of each basin is determined by scaling its relative transgression factor with the global transgression factor (0.77). Basins depicted in the darkest shade of orange especially contribute to the global transgression, with regional land area deviations higher than the global factor. Based on data from [2].

3 PB: Modification of Biogeochemical Flows

Additional information on the global risk map for nitrogen cycle transgression

The global risk map for nitrogen cycle transgression is based on a modification of the methodology presented by Schulte-Uebbing et al. (2022).[3]

Both the critical nitrogen deposition rates and the critical nitrogen concentration in surface waters are defined by a lower and an upper threshold, allowing the calculation of a spatially explicit zone of increasing risk. Consistent with Steffen et al. (2015), the lower and upper thresholds for critical nitrogen concentration in surface waters are 1.0 and 2.5 mg N L^{-1}, respectively. The lower and upper thresholds for critical nitrogen deposition were adopted from Table S2 in Schulte-Uebbing et al. (2022). For biomes for which only a single threshold value was reported, this value was used as the upper deposition threshold.

When aggregated globally, these thresholds correspond to a safe boundary of 37.1 Mt N yr^{-1} for nitrogen surplus and a high-risk threshold of 67.1 Mt N yr^{-1}. In comparison, the threshold values used by Schulte-Uebbing et al. (2022) yield a single boundary of 61 Mt N yr^{-1}. These values are broadly consistent with those reported in Table S5 of Röckström et al. (2023)[4], which estimates a safe boundary of 34 Mt N yr^{-1} and a high-risk threshold of 74 Mt N yr^{-1} for 2010.

4 PB: Land System Change

Additional information on the assessment of the Land System Change Planetary Boundary

We quantify land-system change as loss of contiguous forest relative to potential natural forest. Potential forest is taken from the potential vegetation map by Ramankutty and Foley [5] (5 arc-min), while annual observed forest is provided by ESA/C3S land-cover products (300 m; ESA v2.0.7 for 1992-2015 and C3S v2.1.1 for 2016-2022) [6]. First, annual ESA layers are read, then aggregated to 5 arc-min by modal class to match the potential-forest grid; an additional 30 arc-min product is created to map the 2022-1992 forest-cover change. This maps the percentage-point difference of 5 arc-min forest cells within the larger 30 arc-min grid, capped to [-10, 10].

Next, potential forest is partitioned into tropical, temperate, and boreal. All clearly defined classes are directly assigned from Ramankutty; mixed forest (class 8) is split into temperate vs boreal using CHELSA annual average temperature (aggregated/resampled), with a 6°C threshold. Contiguous-biome polygons are then applied to define major regional forest systems (Fig.1). This means that forest cover outside the biome specific extent does not count for the boundary status (e.g. North-American temperate forest within the boreal region polygon), based on the argument that only large contiguous forests can have Earth-system-wide impacts [7]. With every pixel counting only for one unique biome - forest type - combination (e.g. Eurasia boreal), double counting for overlapping polygons is prevented.

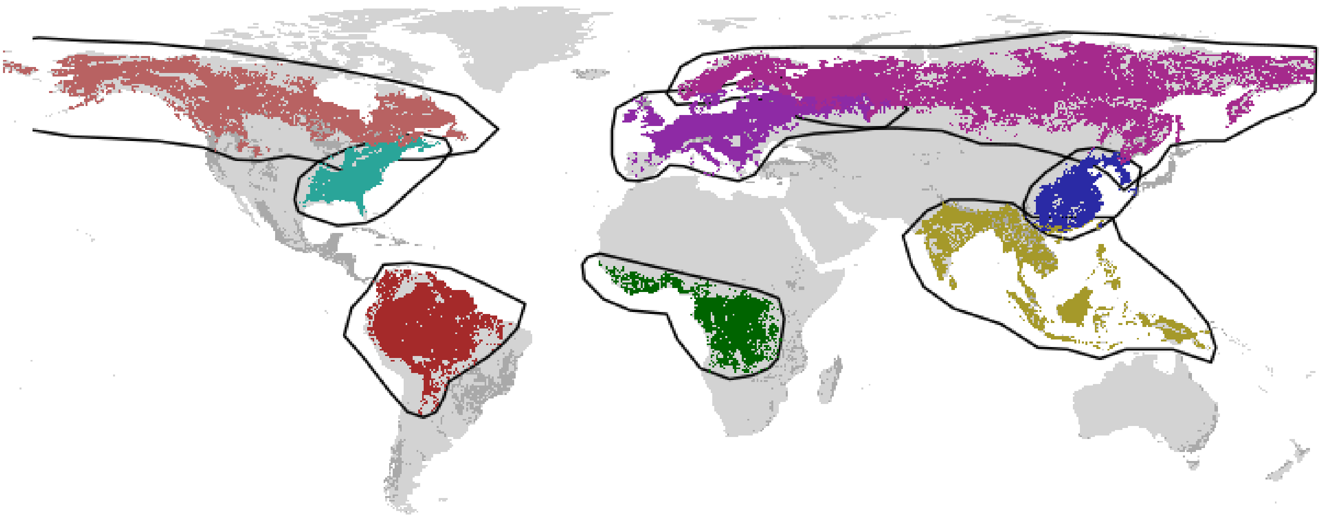

Figure 1: Contiguous biome shapes delineating the extent in which potential and actual forest cover counts towards the boundary. These shapes are expert based and used since Steffen et al. 2015 [7].

For each year and biome polygon, we compute potential forest area and remaining forest area (km2), where remaining forest is derived from selected ESA forest classes (closed and closed-to-open classes plus mixed and mangroves). The planetary boundary control variable, globally remaining forest in percent of potential forest, is computed from the respective sums of all forest cover data from the biome level.

To assess the planetary boundary status, biome-specific thresholds are applied: Holocene baseline (100%), safe threshold (temperate 50%, tropical 85%, boreal 85%), and high-risk threshold (temperate 30%, tropical 60%, boreal 60%). The global PB threshold (78%) is computed as an area-weighted average of the biome thresholds (boreal: 19.1 Mkm^2; temperate: 9.9 Mkm^2; tropical: 19.1 Mkm^2). The mapped control variable is transformed to a normalized risk scale between Holocene, PB, and high-risk thresholds via a gradual, perceptually uniform color scheme, and mapped in equal-cylindrical projection. Final outputs include global risk maps (showing all forest areas, and the relevant potential and deforested regions), global and biome wide time-series (1992-2022), and a forest-cover change map between 2022 and 1992.

5 PB: Ocean Acidification

Additional Information on methods and data of the Ocean Acidification Planetary Boundary.

An ensemble of surface ocean carbonate system data products was retrieved and evaluated for the Planetary Health Check (PHC) 2026. Table 5.1 defines the products retrieved and assessed in this analysis by Daniel Ford.

Dataset (Version)	Spatial and Temporal Coverage	Reference + Dataset Location
UExP-FNN-U (v2026-pre1)	Monthly 1 degree (1980 – 2025 **)	(Ford et al., 2024[8]) `https://doi.org/10.5281/zenodo.19605928`
CMEMS-LSCE-FFNN-v2 (v2026-03 *)	Monthly 0.25 degree (1985 – 2024)	(Chau, Chevallier, et al., 2024[9]; Chau, Gehlen, et al., 2024[10]) `https://doi.org/10.48670/moi-00047`
OceanSODAv1 (v2025)	Monthly 1 degree (1982 – 2024)	(Gregor & Gruber, 2021[11]) `https://data.up.ethz.ch/shared/OceanSODA-ETHZv1/v2025/OceanSODA_ETHZ-v2025.OCADS.01-1982-2024.nc`
Jiang et al. (2023) [12] boundary	Decadal 1 degree (1750)	(Jiang et al., 2023[12]) `https://doi.org/10.25921/9ker-bc48`
JMA-MLR (v2025)	Monthly 1 degree (1990 – 2024)	(Iida et al., 2021 [13]) `https://www.data.jma.go.jp/kaiyou/english/co2_flux/co2_flux_data_en.html`

Table 5.1: Full surface ocean carbonate system datasets used within the analysis and the respective versions.
∗ Version that was reported within the CMEMS download application.
∗∗ 2025 is a 'forecast' year, and is not used in the Planetary Health Check 2026.

Each product (Table 5.1) was area-weighted averaged into annual mean aragonite saturation state using the full spatial and temporal resolution of each dataset. The area was weighted using an ocean proportion mask generated from the European Space Agency Land Climate Change Initiative water bodies mask (150 m),[14] for the spatial resolution of each product. The area of each pixel was calculated assuming the Earth is an ellipsoid.

Figure 40 (left panel) in the main text shows the annual aragonite saturation state for each product on their native grid (i.e the geographical coverage of each dataset varies). The ensemble of products shows a relatively large spread in global aragonite saturation state, mainly due to differences in geographical coverage. UExP-FNN-U showed the lowest aragonite saturation state of all the products but had the largest and over the years most consistent coverage.

Previous analysis completed for the PHC 2025 showed that differences between OceanSODAv1 and the UExP-FNN-U could be explained by the different geographical coverages. For example, the UExP-FNN-U covers under-ice regions in the Arctic and Southern Ocean that typically have a lower aragonite saturation state, therefore reducing the annual mean aragonite saturation state. The CMIP6-model-based Jiang et al. (2023) [12] dataset that was used to establish the preindustrial baseline of aragonite saturation state also has incomplete global geographical coverage as it omits the Mediterranean Sea, Red Sea, Hudson Bay, and does not extend into the coastal regions as much as some of the observation-based data products being assessed (Figure 3, left panel).

Therefore, in addition to the analysis in the main text, the four data products were also evaluated on a consistent coverage grid where all products provide an estimate of aragonite saturation state. Note that CMEMS-LSCE-FFNN-v2 was regridded from 0.25 degree to 1 degree. Figure 2 (left) shows the analysis where all products cover the same area, that excludes much of the Arctic Ocean, some of the ice-covered Southern Ocean and the Mediterranean Sea. The UExP-FNN-U and OceanSODAv1 products showed very good consistency when evaluated on a consistent coverage. CMEMS-LSCE-FFNN-v2 showed a reduced aragonite saturation state with values similar to the limits of the UExP-FNN-U 2-sigma uncertainty. The baseline (i.e. the Jiang et al. 2023 [12] value for 1750) and boundary (defined as 80% of the baseline) were also assessed with this refined coverage (i.e. assessed on the consistent geographical coverage), showing that all products breach or got close to breaching the boundary in recent years. This analysis demonstrates that the differences between the data products seen in Figure 40 stem primarily from the different geographical coverage of these products. When aligned to the same spatial extent, the products show much closer agreement.

The analysis for UExP-FNN-U provides uncertainties for the annual aragonite saturation state, as shown in Figure 2 (left). The uncertainty was calculated following the methods of Ford et al. (2024)[8], where the fugacity of CO2 in seawater (fCO2(sw)) uncertainty was identified as the dominant source of uncertainty and therefore the spatial decorrelation for fCO2(sw) was used. No temporal correlation was assumed as in Ford et al. (2024)[8].

5.1 Hydrogen Ion concentration (or pH on the free scale)

The same analysis was conducted for Hydrogen Ion concentrations (i.e the pH on the free scale converted to concentrations) for the three observation-based products and the Jiang et al. (2023) [12] dataset used to assess the baseline and boundary. UExP-FNN-U and ETHZ-OceanSODA provide pH on the free scale as standard. CMEMS-LSCE-FFNN-v2 and JMA-MLR provides the pH on the total scale, which was converted to pH on the free scale using pyCO2SYS (v1.8.3.3; Humphreys et al., 2022 [15]) and the temperature and salinity for each product. Figure 40 (right panel) in the main text shows the free hydrogen ion concentration of the data products on their native geographical coverage, and Figure 2 (right) shows all the products on the same consistent coverage (note: CMEMS-LSCE-FFNN-v2 was regridded from 0.25 degree to 1 degree as in the analysis of aragonite saturation state).

5.2 High-Risk Value of the Ocean Acidification Planetary Boundary

The Planetary Boundaries framework defines a safe operating space and, where scientific evidence allows, a zone of increasing risk extending towards conditions of high risk. For ocean acidification, the Planetary Boundary is set at 80% of the pre-industrial aragonite saturation state. Earlier assessments used 70% of the pre-industrial value as the upper end of the zone of increasing risk. However, the scientific basis for this high-risk level has not been comprehensively reassessed against the growing literature on ocean acidification impacts and Earth-system consequences. A targeted assessment is therefore planned to evaluate and, where possible, update the high-risk value using the latest scientific evidence.

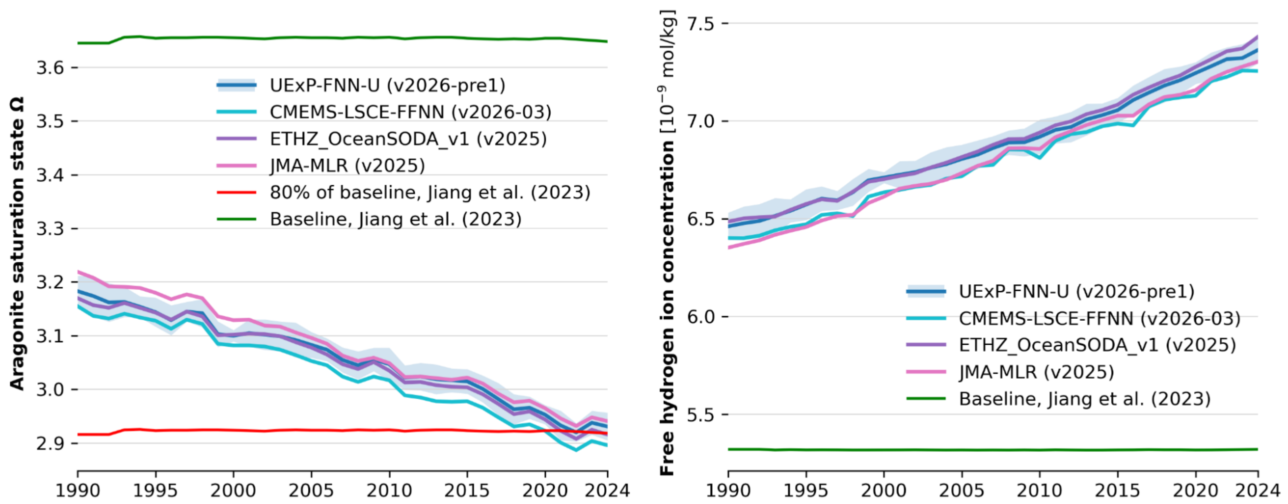

Figure 2: Left: Annual area-weighted mean aragonite saturation state for each product on a consistent coverage (i.e geographical coverage where all products have estimates). The consistent coverage is also applied to the baseline (green), i.e. the year 1750 from Jiang et al. (2023).[12] For that reason, the baseline also changes slightly over time. A line for 80% of the baseline (red) is shown to reflect the boundary value if it was evaluated on the consistent coverage. Banding around UExP-FNN-U (v2026-pre1) indicates the 2 sigma uncertainty based on spatial and temporal correlation uncertainty propagation approach described in Ford et al. (2024)[8]. Right: Same as the left panel, but for the annual area-weighted mean concentration of free hydrogen ions for each product on a consistent coverage. No line reflecting the boundary value is shown, as no boundary is defined for the concentration of free hydrogen ions.

5.3 Ocean Warming

The ocean has been warming for as long as comprehensive measurements have taken place (the late 1950s / early 1960s). It is estimated that approximately 90% of the excess heat trapped by anthropogenic greenhouse gas emissions is ultimately taken up by the ocean,[16, 17] resulting in dramatically lower warming in the atmosphere

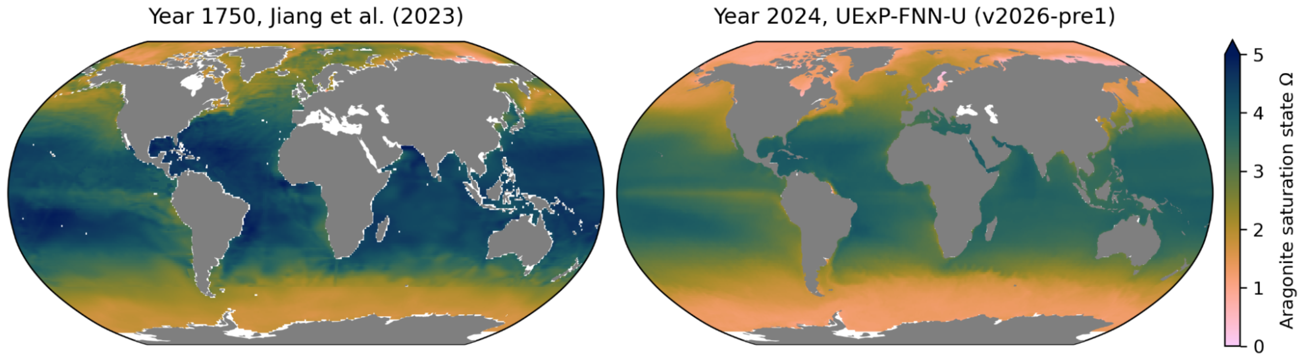

Figure 3: Maps of the absolute aragonite saturation state for the preindustrial baseline (left), based on the year 1750 from Jiang et al. (2023),[12] and for the present day (right), based on the year 2024 from the UExP-FNN-U (v2026-pre1) dataset. Both maps use an identical color scale indicated on the right.

and on land.

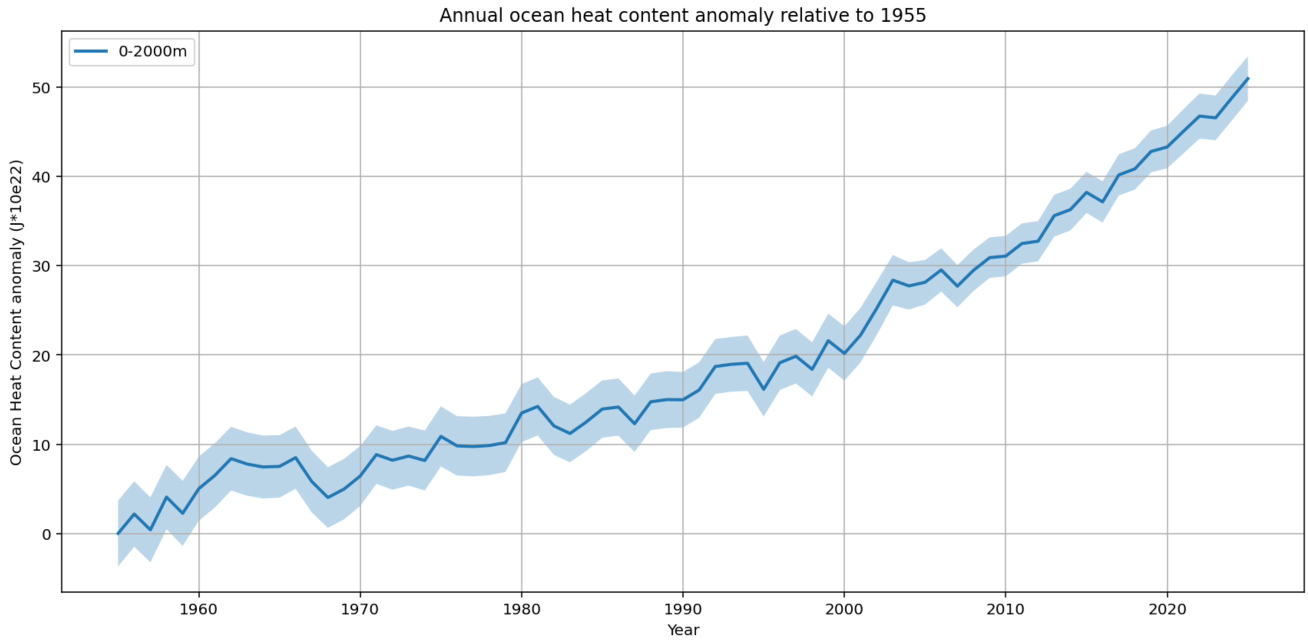

Figure 4: Integrated ocean heat content anomaly in the top 2000 m referenced to 1955. Data taken from the Japanese Meteorological Agency (`https://www.data.jma.go.jp/kaiyou/english/ohc/ohc_global_en.html`)

There is recent evidence showing that the rate of ocean warming has accelerated over the 21st century [18] at a rate almost twice as fast as that during the 20th century. In 2025, ocean heat content increased by a record 23 +- 8 Zetta Joules,[19] or roughly 12 nuclear bombs exploding in the ocean every second.

Bibliography

1. Lehner, B. & Grill, G. Global river hydrography and network routing: baseline data and new approaches to study the world's large river systems. en. *Hydrological Processes* **27,** 2171–2186 (2013).
2. Virkki, V., Andersen, L. S., Te Wierik, S., Gerten, D. & Porkka, M. Regionally divergent drivers behind transgressions of the freshwater change planetary boundary. en. *Nature Communications* **17,** 5132 (2026).
3. Schulte-Uebbing, L. F., Beusen, A. H. W., Bouwman, A. F. & de Vries, W. From planetary to regional boundaries for agricultural nitrogen pollution. en. *Nature* **610,** 507–512 (2022).
4. Rockström, J. *et al.* Safe and just Earth system boundaries. en. *Nature* **619.** Number: 7968, 102–111 (2023).
5. Ramankutty, N. & Foley, J. A. Estimating historical changes in global land cover: Croplands from 1700 to 1992. en. *Global Biogeochemical Cycles* **13,** 997–1027 (1999).
6. Copernicus Climate Change Service (C3S) Climate Data Store (CDS). *Land cover classification gridded maps from 1992 to present derived from satellite observation* 2024.
7. Steffen, W. *et al.* Planetary boundaries: Guiding human development on a changing planet. *Science* **347,** 1259855 (2015).
8. Ford, D. J. *et al.* A Comprehensive Analysis of Air-Sea CO2 Flux Uncertainties Constructed From Surface Ocean Data Products. en. *Global Biogeochemical Cycles* **38,** e2024GB008188 (2024).
9. Chau, T.-T.-T., Chevallier, F. & Gehlen, M. Global Analysis of Surface Ocean CO_2 Fugacity and Air-Sea Fluxes With Low Latency. en. *Geophysical Research Letters* **51,** e2023GL106670 (2024).
10. Chau, T.-T.-T., Gehlen, M., Metzl, N. & Chevallier, F. CMEMS-LSCE: a global, 0.25°, monthly reconstruction of the surface ocean carbonate system. en. *Earth System Science Data* **16,** 121–160 (2024).
11. Gregor, L. & Gruber, N. OceanSODA-ETHZ: a global gridded data set of the surface ocean carbonate system for seasonal to decadal studies of ocean acidification. English. *Earth System Science Data* **13,** 777–808 (2021).
12. Jiang, L.-Q. *et al.* Global Surface Ocean Acidification Indicators From 1750 to 2100. en. *Journal of Advances in Modeling Earth Systems* **15,** e2022MS003563 (2023).
13. Iida, Y., Takatani, Y., Kojima, A. & Ishii, M. Global trends of ocean CO2 sink and ocean acidification: an observation-based reconstruction of surface ocean inorganic carbon variables. en. *Journal of Oceanography* **77,** 323–358 (2021).
14. Lamarche, C. *et al.* Compilation and Validation of SAR and Optical Data Products for a Complete and Global Map of Inland/Ocean Water Tailored to the Climate Modeling Community. en. *Remote Sensing* **9,** 36 (2017).
15. Humphreys, M. P., Lewis, E. R., Sharp, J. D. & Pierrot, D. PyCO2SYS v1.8: marine carbonate system calculations in Python. English. *Geoscientific Model Development* **15,** 15–43 (2022).
16. Von Schuckmann, K. *et al.* Heat stored in the Earth system: where does the energy go? English. *Earth System Science Data* **12,** 2013–2041 (2020).
17. Cheng, L., Foster, G., Hausfather, Z., Trenberth, K. E. & Abraham, J. Improved Quantification of the Rate of Ocean Warming. EN. *Journal of Climate* **35,** 4827–4840 (2022).
18. Minière, A., von Schuckmann, K., Sallée, J.-B. & Vogt, L. Robust acceleration of Earth system heating observed over the past six decades. en. *Scientific Reports* **13,** 22975 (2023).
19. Pan, Y. *et al.* Ocean Heat Content Sets Another Record in 2025. en. *Advances in Atmospheric Sciences* (2026).